

Comparison of *P*-wave attenuation models of wave-induced flow

Weitao Sun¹, Jing Ba^{2*}, Tobias M. Müller³, José M. Carcione⁴ and Hong Cao²

¹Zhou Pei-Yuan Center for Applied Mathematics, Tsinghua University, Beijing 100084, China, ²Geophysical Department, RIPED, PetroChina, Beijing 100083, China, ³CSIRO Energy Flagship, Kensington, WA 6151, Australia, and ⁴Istituto Nazionale di Oceanografia e di Geofisica Sperimentale, 34010 Trieste, Italy

Received December 2012, revision accepted May 2014

ABSTRACT

Wave-induced oscillatory fluid flow in the vicinity of inclusions embedded in porous rocks is one of the main causes for *P*-wave dispersion and attenuation at seismic frequencies. Hence, the *P*-wave velocity depends on wave frequency, porosity, saturation, and other rock parameters. Several analytical models quantify this wave-induced flow attenuation and result in characteristic velocity–saturation relations. Here, we compare some of these models by analyzing their low- and high-frequency asymptotic behaviours and by applying them to measured velocity–saturation relations. Specifically, the Biot–Rayleigh model considering spherical inclusions embedded in an isotropic rock matrix is compared with White’s and Johnson’s models of patchy saturation. The modeling of laboratory data for tight sandstone and limestone indicates that, by selecting appropriate inclusion size, the Biot–Rayleigh predictions are close to the measured values, particularly for intermediate and high water saturations.

Key words: *P*-wave dispersion/attenuation, Double porosity, Biot–Rayleigh theory, Local fluid flow, Patchy saturation.

INTRODUCTION

Wave-induced local fluid flow causes attenuation and velocity dispersion in fluid-saturated rocks (Dvorkin and Nur 1993; Müller, Gurevich, and Lebedev 2010). This is because energy is dissipated through the relative motion between the solid skeleton and fluid phases. Dispersion and attenuation depend on several factors such as the saturating fluids, the fluid distribution patterns (patch size and shape), and pore heterogeneity (Cadoret, Mavko, and Zinszner 1998; Müller and Gurevich 2004; Toms, Müller, and Gurevich 2007; Caspari, Müller, and Gurevich 2011). The loss mechanism is also related to the type of flow. Global flow attenuation was predicted by Biot (1962). Although Biot mentioned the local fluid flow, a predictive theory was not established until the 1970s (White 1975; White, Mikhaylova, and Lyakhovitskiy 1975; Dutta and Odé 1979a, b; Dutta and Seriff 1979). On the other hand, the mesoscopic loss mechanism is believed to describe the attenuation at seismic frequencies (Ba *et al.* 2008; Ba, Car-

cione, and Nie 2011). This mechanism is inherently frequency dependent. Even for the same type of pore structure and saturation, the elastic response of rocks will show different behaviours at low and high frequencies (Carcione 2007a).

A heterogeneous pore structure and/or fluid distribution may stiffen or soften the rock at different frequency bands (Cadoret, Marion, and Zinszner 1995; Carcione and Helle 2002; Ruiz and Ilgar Azizov 2011). In the case of multiple fluids, the effective fluid bulk modulus K_w is given by Wood’s law at low frequencies, i.e., when the fluid pore pressure is uniform between patches. It can be used together with the Biot–Gassmann equation to predict wave velocity (Biot–Gassmann–Wood or BGW theory) (Toms *et al.* 2007). At high frequencies, there is no time for fluid pressure equilibration between fluid patches (White 1975; Dutta and Odé 1979a, b; Johnson 2001). The wet-rock bulk modulus is constant only within each patch, and the shear modulus is not affected. Invoking Hill’s theory (Hill 1963, 1964), the effective bulk modulus K_H of the composite can be obtained. The so-called

*E-mail: baj08@petrochina.com.cn

Biot–Gassmann–Hill (BGH) formula yields a good estimate of the velocity at high frequencies (Toms *et al.* 2007).

The BGW and BGH theories predict the effective bulk modulus at the low and high frequency limits. At intermediate frequencies, the diffusion wavelength is comparable to the size of the fluid patch. There are several approaches to model the mesoscopic velocity dispersion and the related attenuation mechanism (Sun *et al.* 2012). White (1975) considered spherical gas pockets in a water-saturated porous medium. He also considered porous layers alternately saturated with water and gas (White *et al.* 1975). The effects of fluid flow across boundaries on P -wave dispersion and attenuation were quantified. Dutta and Odé (1979) improved White's spherical patchy saturation model by using Biot's theory (Dutta and Seriff 1979). More recently, Johnson (2001) developed a generalization of White's model for patches of arbitrary shape by using a branching function approach (Johnson 2001). Carcione and Picotti (2006) studied the influence of the fluid properties and frame (matrix) properties on the dispersion/attenuation curves (Carcione and Picotti 2006). Recently, Ba *et al.* (2011) have formulated a double-porosity model based on the flow dynamics theory developed by Rayleigh (1917), where the local fluid flow of a spherical inclusion is modeled. Dynamic equations for double-porosity media are obtained, and the effective bulk modulus is calculated.

In this work, the Biot–Rayleigh (BR) theory (Ba *et al.* 2011) is adapted to the case of patchy-saturated rocks, where gas is an inclusion in a water-saturated background medium. The contrasts in density, viscosity, and bulk modulus between the gas- and water-saturated zones constitute mesoscopic heterogeneities, i.e., the inclusions radii are much smaller than the P -wavelength but larger than the pore size. Thus, the partially saturated rock can be considered a special case of a double-porosity medium with regions of different compliances. Based on this double-porosity model (Ba *et al.* 2011; Ba *et al.* 2012), the dispersion/attenuation curves are calculated and compared with those of White's and Johnson's models (White 1975; Johnson 2001).

LAGRANGIAN EQUATION FOR PATCHY-SATURATED MEDIA

The BR model consists of spherical inclusions embedded in a homogeneous host medium. It is applicable in two cases: a single-porosity solid saturated with two immiscible fluids and a double-porosity solid saturated with a single type of fluid (Ba *et al.* 2013). The inclusions are homogeneous, and their

radii are much smaller than the P -wavelength but larger than the pore size (i.e., mesoscopic).

The wave-induced flow is caused by mesoscopic-scale heterogeneity, which is modeled as a mixture of two porous phases saturated by a single fluid in the BR model. A double-porosity solid can be envisioned in many ways. For example, there can be a small volume fraction of less consolidated sand grains in an apparently uniform sandstone formation. Strongly dissolved dolomite is another example, in which powder crystals are present in the pores forming a second matrix. The main difference between single- and double-porosity solids is that the mineral grain frame is homogeneous in porosity and compressibility in a single-porosity solid. For the case of a single-porosity solid saturated with two immiscible fluids (for instance, a rock partially saturated with gas and water), the inclusions are gas pockets (or water pockets) while the host medium of porous rock is saturated with water (or gas), and the inclusions and host medium have the same skeleton if it is treated with the BR theory. The pores between the inclusion and the host medium are open, and the inclusions are assumed isolated from each other so that the interaction between them can be ignored. In isotropic double-porosity media, the strain energy density can be expressed as (Ba *et al.* 2011):

$$W = \frac{1}{2}[(A + 2N)I_1^2 - 4NI_2 + 2Q_1I_1(\varepsilon_1 + \phi_2\zeta) + R_1(\varepsilon_1 + \phi_2\zeta)^2 + 2Q_2I_1(\varepsilon_2 - \phi_1\zeta) + R_2(\varepsilon_2 - \phi_1\zeta)^2]. \quad (1)$$

Here $I_1 = e_{11} + e_{22} + e_{33}$ and $I_2 = \begin{vmatrix} e_{11} & e_{12} \\ e_{21} & e_{22} \end{vmatrix} + \begin{vmatrix} e_{22} & e_{23} \\ e_{32} & e_{33} \end{vmatrix} + \begin{vmatrix} e_{33} & e_{31} \\ e_{32} & e_{32} \end{vmatrix}$ are the first and second strain invariants of solid matrix displacement \mathbf{u} . The strain components are defined as $e_{ij} = \frac{1}{2}(u_{i,j} + u_{j,i})$. Moreover, $\varepsilon_m = \xi_{11}^{(m)} + \xi_{22}^{(m)} + \xi_{33}^{(m)}$ are the first strain invariants of the average fluid displacement $\mathbf{U}^{(m)}$ in the two porosity systems, with $\xi_{ij}^{(m)} = \frac{1}{2}(U_{i,j}^{(m)} + U_{j,i}^{(m)})$. Here $m = 1, 2$ represent the displacements in the host medium and inclusion, respectively (they represent the two fluid phases in the case of a single-porosity matrix saturated with two fluids); ϕ_1 and ϕ_2 are the absolute porosity of the host medium and inclusion (it is the absolute porosity for each fluid phase in partially saturated medium), $\zeta = \frac{1}{\phi_1}(1 - \frac{R_0^3}{R^3})$ is the variation of fluid content, inclusion size R is the dynamic radius of the spherical inclusion at the boundary at time t , R_0 is the initial value of R , and N is the shear modulus of the frame. The coefficients A , Q_m , R_m ($m = 1, 2$) are the stiffness values, which are functions of the porosity ϕ , the frame bulk modulus K_b , and the solid's and two fluid's bulk

moduli K_s, K_{f_m} . A is the effective elastic parameter of the solid phase. R_1 and R_2 are effective elastic parameters of fluid phase. Q_1 and Q_2 represent the solid–fluid coupling strength modulus. The explicit expressions for the four Biot elastic parameters of a single-porosity medium have been derived by three “gedanken” experiments (Johnson 1986). In the same manner, idealized experiments can be performed for a double-porosity medium. (i) The material is subjected to a pure shear deformation. (ii) The rock sample is surrounded by a flexible rubber jacket, subjected to a hydrostatic pressure, and the pore fluid is allowed to flow in and out. (iii) The rock sample is subjected to a uniform hydrostatic pressure, and the mineral grain is homogeneous and isotropic. Applying the stress–strain relations from strain energy function to idealized experiments, the expressions of the stiffness coefficients can be obtained (Ba *et al.* 2011).

The kinetic energy density of the double-porosity medium is (Ba *et al.* 2011):

$$T = \frac{1}{2} \left[\rho_{00} \sum_{i=1}^3 \dot{u}_i^2 + 2 \sum_{m=1}^2 \rho_{0m} \sum_{i=1}^3 \dot{u}_i \dot{U}_i^{(m)} + \sum_{m=1}^2 \rho_{mm} \sum_{i=1}^3 (\dot{U}_i^{(m)})^2 \right] + 2T_L, \quad (2)$$

where

$$\begin{aligned} \rho_{00} &= \left(1 - \sum_{m=1}^2 \phi_m \right) \rho_s - \sum_{m=1}^2 \rho_m + \sum_{m=1}^2 \rho_{mm} \\ \rho_{0m} &= \rho_m - \rho_{mm}, \quad \rho_{mm} = \alpha_m \phi_m \rho_{f_m} \\ \rho_m &= \phi_m \rho_{f_m}, \quad \phi_m = v_m \phi_0, \quad (m = 1, 2). \end{aligned} \quad (3)$$

The host and inclusion densities are $\rho_m = \phi_0 \rho_{f_m}$ ($m = 1, 2$), where ρ_s, ρ_{f_m} are the solid and the two fluid’s mass densities, and v_m is the volume fraction of fluid zone m . The porosity of the whole inclusion is ϕ_0 . The tortuosity is given as $\alpha_m = \frac{1}{2} (1/\phi_{m0} + 1)$ (Berryman 1979).

The kinetic energy density T_L related to compression deformations is (Ba *et al.* 2011):

$$T_L = \frac{1}{6} \left(\frac{\phi_1^2 \phi_2 \phi_{20}}{\phi_{10}} \right) \rho_{f_1} R_0^2 \xi^2. \quad (4)$$

In the above formula, $\phi_m = v_m \phi_{m0} = v_m \phi_0$ ($m = 1, 2$) since we assume that the inclusions and host medium share the same pore structures; moreover, they have the same permeability κ .

Biot’s dissipation function and local fluid flow dissipation functions are (Ba *et al.* 2011):

$$D = \frac{1}{2} \sum_{m=1}^2 b_m \dot{\mathbf{w}}^{(m)} \cdot \dot{\mathbf{w}}^{(m)}, \quad (5)$$

$$D_L = \frac{1}{6} \left(\frac{\eta_1}{\kappa} \right) \phi_1^2 \phi_2 \phi_{20} R_0^2 \xi^2. \quad (6)$$

Here $\mathbf{w}^{(m)} = \phi_m (\mathbf{U}^{(m)} - \mathbf{u}^{(m)})$ and $b_m = \phi_m \phi_0 \left(\frac{\eta_m}{\kappa} \right)$. η_m ($m = 1, 2$) are the fluid viscosities. The Lagrangian formulation of equations of motion for the current system is given by Achenbach (1987) and Ba *et al.* (2011):

$$\frac{\partial}{\partial t} \left(\frac{\partial L}{\partial \dot{q}_j} \right) + \sum_{k=1}^3 \frac{\partial}{\partial q_k} \left[\frac{\partial L}{\partial q_{j,k}} \right] + \frac{\partial (D + D_L)}{\partial \dot{q}_j} = \frac{\partial L}{\partial q_j}, \quad (7)$$

with $L = T - W$. The q_j ’s are generalized coordinates and represent the components of $(u_i, U_i^{(m)}, \zeta)$ ($m = 1, 2, i = 1, 2, 3$).

The above Lagrangian formula leads to the following dynamic equations (Ba *et al.* 2011):

$$\begin{aligned} N \nabla^2 \mathbf{u} + (A + N) \nabla I_1 + Q_1 \nabla (\varepsilon_1 + \phi_2 \zeta) + Q_2 \nabla (\xi_2 - \phi_1 \zeta) \\ = \rho_{00} \ddot{\mathbf{u}} + \sum_{m=1}^2 [\rho_{0m} \ddot{\mathbf{U}}^{(m)} + b_m (\ddot{\mathbf{u}} - \dot{\mathbf{U}}^{(m)})], \end{aligned} \quad (8)$$

$$Q_1 \nabla I_1 + R_1 \nabla (\varepsilon_1 + \phi_2 \zeta) = \rho_{01} \ddot{\mathbf{u}} + \rho_{11} \ddot{\mathbf{U}}^{(1)} + b_1 (\dot{\mathbf{U}}^{(1)} - \dot{\mathbf{u}}), \quad (9)$$

$$Q_2 \nabla I_1 + R_2 \nabla (\varepsilon_2 - \phi_1 \zeta) = \rho_{02} \ddot{\mathbf{u}} + \rho_{22} \ddot{\mathbf{U}}^{(2)} + b_2 (\dot{\mathbf{U}}^{(2)} - \dot{\mathbf{u}}), \quad (10)$$

$$\begin{aligned} \phi_2 Q_1 I_1 + \phi_2 R_1 (\varepsilon_1 + \phi_2 \zeta) - \phi_1 Q_2 I_1 - \phi_1 R_2 (\varepsilon_2 - \phi_1 \zeta) \\ = \left(\frac{\rho_f}{\phi_0} \ddot{\zeta} + \frac{\eta_1}{\kappa} \dot{\zeta} \right) \frac{\phi_1^2 \phi_2}{3} R_0^2 \phi_0. \end{aligned} \quad (11)$$

This system of coupled equations has ten unknowns ($u_i, U_i^{(m)}, \zeta, i = 1, 2, 3, m = 1, 2$). It entails six stiffness values (A, N, Q_m, R_m), five density coefficients ($\rho_{00}, \rho_{0m}, \rho_{mm}$), three geometrical coefficients (ϕ_m, R), the transport properties κ , and the fluid viscosity η_m . The stiffness and density coefficients have been discussed and quantitatively estimated on the basis of measurable properties of solid and fluids ($\phi_0, K_s, N, K_{f_1}, K_{f_2}, K_b, \rho_s, \rho_{f_1}, \rho_{f_2}$). The geometrical coefficient R represents the radius of sphere inclusion, indicating the size of gas pockets if the rock is treated as a single-porosity medium saturated with two immiscible fluids (gas and water).

White (1975) developed the patchy saturation theory for an elastic porous solid saturated with two immiscible fluids. The idealized geometry contains a gas pocket that is located at

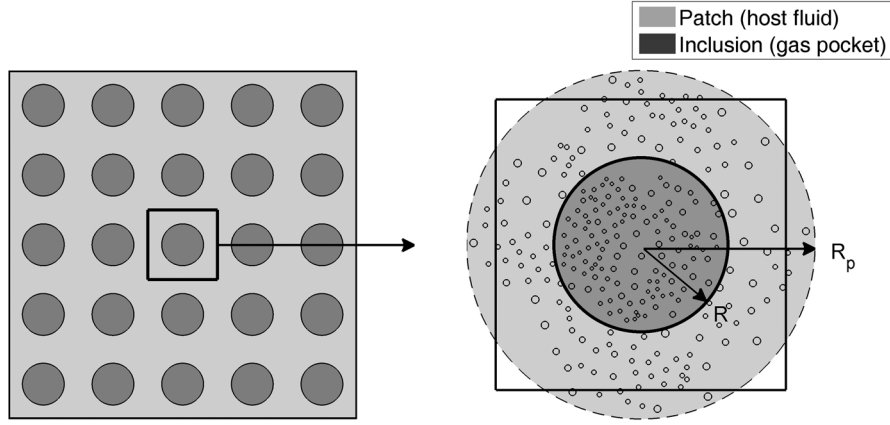


Figure 1 The inclusion and patch geometry. According to White (1975), each cubic unit in the medium contains a sphere inclusion in the centre. The cubic unit is treated as an outer sphere with the same volume. R_p represents the patch radius. The ratio of $(R/R_p)^3$ gives saturation.

the center of each cubic unit (Fig. 1) in a periodical array system. The concentric spheres are considered where the volume of the outer sphere is equal to the volume of each single unit cube. The inner spherical pocket is the inclusion (gas pocket), and the whole volume of the outer sphere is the patch.

X-ray computer tomography has been used to reveal fluid distribution inside the rock sample during saturation (Lebedev *et al.* 2009). The resolution is not sufficient to image the exact fluid patch geometry; however, it shows the overall character of the fluid distribution. The patch size is not uniform in real rock saturation. An effective or average size can be used to reflect the influence of patchy saturation.

The stiffness coefficients can be derived through idealized experiments (Ba *et al.* 2011). Following the calculations of density coefficients proposed by Biot (Johnson 1986), the formulas for density coefficients can be derived. Assuming that there is no relative motion between fluid and solid ($u_i = U_i^{(m)}$), the pressure difference in the fluid per unit length is $-\phi_m \nabla_i p = \phi_m \rho_{f_m} \frac{\partial^2 u_i}{\partial t^2}$ or $Q_i^{(m)} = \phi_m \rho_{f_m} \frac{\partial^2 u_i}{\partial t^2}$. From Lagrange's equations, we have $Q_i^{(m)} = \frac{\partial}{\partial t} \left(\frac{\partial T}{\partial U_i^{(m)}} \right) = (\rho_{0m} + \rho_{mm}) \frac{\partial^2 u_i}{\partial t^2}$. Comparing the above equations, we derive:

$$\phi_m \rho_{f_m} = \rho_{0m} + \rho_{mm}, \quad m = 1, 2. \quad (12)$$

Since $u_i = U_i^{(m)}$, the kinetic energy becomes $T = \frac{1}{2} \sum_{i=1}^3 (\rho_{00} + 2 \sum_{m=1}^2 \rho_{0m} + \sum_{m=1}^2 \rho_{mm}) \dot{u}_i^2$.

The total mass of fluid–solid aggregate per unit volume is $\rho = \rho_{00} + 2 \sum_{m=1}^2 \rho_{0m} + \sum_{m=1}^2 \rho_{mm}$. The total density can also be expressed by $\rho = \rho_0 + \sum_{m=1}^2 \phi_m \rho_{f_m} = \rho_0 +$

$\sum_{m=1}^2 (\rho_{0m} + \rho_{mm})$, where ρ_0 is the density of grain skeleton. Comparing the above equations, we derive:

$$\rho_0 = \rho_{00} + \sum_{m=1}^2 \rho_{0m}. \quad (13)$$

The tortuosity α is the mean square deviation of the microscopic field of the solid from the solid mean field, normalized by the square of the relative field between the solid and fluid constituents (Carcione 2007b). In terms of the tortuosity, the density coefficient ρ_{mm} can be written as (Berryman 1980):

$$\rho_{mm} = \tau^{(m)} \phi_m \rho_{f_m}, \quad m = 1, 2, \quad (14)$$

where $\tau^{(m)} = \frac{1}{2} \left(1 + \frac{1}{\phi_{m0}} \right)$. We have five unknowns $\rho_{00}, \rho_{0m}, \rho_{mm}$ ($m = 1, 2$) and five equations. Thus, the density coefficients can be determined as:

$$\rho_{mm} = \frac{\rho_{f_m}}{2} \phi_m \left(1 + \frac{1}{\phi_{m0}} \right), \quad (15)$$

$$\rho_{0m} = \frac{\rho_{f_m}}{2} \phi_m \left(1 - \frac{1}{\phi_{m0}} \right), \quad (16)$$

$$\rho_{00} = \rho_0 - \frac{1}{2} \sum_{m=1}^2 \rho_{f_m} \phi_m \left(1 - \frac{1}{\phi_{m0}} \right). \quad (17)$$

Using harmonic analysis of plane waves $u = u_0 e^{i(\omega t - k \cdot x)}$ and $U^{(m)} = U_0^{(m)} e^{i(\omega t - k \cdot x)}$ in the above dynamic equations, we obtain equations for the complex wavenumbers k of the P-wave:

$$\begin{bmatrix} a_{11}k^2 + b_{11} & a_{12}k^2 + b_{12} & a_{13}k^2 + b_{13} \\ a_{21}k^2 + b_{21} & a_{22}k^2 + b_{22} & a_{23}k^2 + b_{23} \\ a_{31}k^2 + b_{31} & a_{32}k^2 + b_{32} & a_{33}k^2 + b_{33} \end{bmatrix} \begin{pmatrix} \mathbf{u} \\ \mathbf{U}^{(1)} \\ \mathbf{U}^{(2)} \end{pmatrix} = 0, \quad (18)$$

where coefficients a_{ij}, b_{ij} are functions of wave frequency ω , rock parameters ($\phi_0, K_s, N, K_{f_1}, K_{f_2}, K_b, \rho_s, \rho_{f_1}, \rho_{f_2}$), and inclusion size R . The definitions of a_{ij}, b_{ij} can be found in (Ba *et al.* 2011). For the sake of simplicity, we will not list the formulas here.

Since the solid and fluid displacements are arbitrary, the determinant of coefficients matrix must be zero, which yields the dispersion relations between ω and k :

$$\begin{vmatrix} a_{11}k^2 + b_{11} & a_{12}k^2 + b_{12} & a_{13}k^2 + b_{13} \\ a_{21}k^2 + b_{21} & a_{22}k^2 + b_{22} & a_{23}k^2 + b_{23} \\ a_{31}k^2 + b_{31} & a_{32}k^2 + b_{32} & a_{33}k^2 + b_{33} \end{vmatrix} = 0. \quad (19)$$

As a consequence, the P -wave dispersion/attenuation can be represented by a complex velocity $v = \omega/k$ and complex plane-wave modulus M^* (Dutta and Odé 1979a):

$$v_p = [\text{Re}(v^{-1})]^{-1}, \quad \alpha(f) = 54.58 \tan(\theta^*/2), \quad (20)$$

$$\tan \theta^*(\omega) = M_I^*(\omega)/M_R^*(\omega). \quad (21)$$

Here M_I^*, M_R^* are the imaginary and real parts of M^* . To predict the P -wave velocity, one needs the following parameters: $\phi_0, K_s, N, K_{f_1}, K_{f_2}, K_b, \rho_s, \rho_{f_1}, \rho_{f_2}, \kappa, \eta_m$, and patch size R_p . The velocity $v = \omega/k$ is numerically calculated as the solutions of equation (19).

The BR model has been verified by numerical examples with a single set of rock parameters, and the P -wave velocity and attenuation have been shown to be functions of frequency (Ba *et al.* 2011). Here, we test the BR model with more data, namely, Casino Otway basin sandstone (Lebedev *et al.* 2009), French Vosgian sandstone (Bacri and Salin 1986), and high-porosity Estailades limestone (Cadoret *et al.* 1995). The predicted P -wave velocities are represented as a function of frequency and water saturation. In addition, we apply the BR model to oil–water saturation, with oil/water being treated as inclusions/host.

REVISED WHITE'S MODEL AND JOHNSON'S MODEL

White (1975) studied P -wave dispersion/attenuation in unconsolidated rocks with partial gas saturation. The energy loss mechanism is based on a spherical gas pocket embedded in a concentric water sphere (White 1975). As a compressional wave travels through such rock with mixed saturation, pressure gradients are high near the inhomogeneities. Fluid flow will be high at these local spots and induce high attenuation. White's work ascribed the P -wave dispersion and attenuation to fluid flow at the mesoscopic level, and this is considered the

first patchy saturation model. Idealized concentric sphere geometry is adopted in White's work. The spherical gas pocket is located at the inner part of the concentric model, which is elsewhere saturated with liquid (see Fig. 1). On the outer surface, a specified fractional volume change is impressed at a low frequency. The resulting pressure amplitude at the surface is computed. Since the effects of fluid flow in the spherical shell are included, the gas pocket provides a complete pressure release. The ratio of pressure amplitude to the fractional volume change yields the complex bulk modulus (White 1975)

$$K^* = \frac{K_0}{1 - K_0 W}, \quad (22)$$

where $W = \frac{3a^2(\Re_1 - \Re_2)(-\Theta_1 + \Theta_2)}{b^3 \omega (Z_1 + Z_2)}$ is a function of the gas pocket radius a and water sphere radius b , acoustic impedance Z_1 and Z_2 of the diffusion waves, wave frequency ω , and other factors such as the porosity, bulk moduli of the contents, etc. K_0 is the average bulk modulus of the two concentric spherical bodies in the absence of fluid flow. Here, $\iota = \sqrt{-1}$. The definition of the coefficients ($\Re_1, \Re_2, \Theta_1, \Theta_2, Z_1, Z_2$) can be found in White's original paper (White 1975). For the sake of convenience of reference, we list the most important formulas in Appendix A. With the shear modulus $N^* = \bar{N}$ (fluid content not affecting shear modulus \bar{N}), the composite density $\rho^* = \rho_0 = (1 - \phi)\rho_s + \phi(1 - S_G)\rho_f$, and the complex bulk modulus K^* , we can calculate the P -wave velocity and attenuation (White 1975), where ρ_s is the mineral grain density, ρ_f is the liquid density, S_G is the gas saturation

$$v_p^* = \frac{\sqrt{|K^* + \frac{4}{3}N^*|/\rho^*}}{\cos(\theta_p^*/2)}, \quad (23)$$

$$\alpha_p^* = \frac{\omega \tan(\theta_p^*/2)}{v_p^*}, \quad (24)$$

$$\theta_p^* = \tan^{-1} \left(\frac{\text{Im}(K^* + \frac{4}{3}N^*)}{\text{Re}(K^* + \frac{4}{3}N^*)} \right) \quad (25)$$

Based on White's patchy model, Dutta *et al.* (1979a) developed the theory of seismic wave dispersion/attenuation in a more rigorous manner. When a plane wave propagates in a homogeneous medium, motions perpendicular to the plane-wave front are expected (Dvorkin and Nur 1993; Dvorkin, Mavko, and Nur 1995). Radial displacements of the fluid and solid material are involved in the deformations from radial stress applied to the outer boundary of the spherical unit cell. Dutta *et al.* (1979a) observed that the P -wave velocity computed by White's method is not correct at the zero-frequency limit

and proposed a correction (Dutta and Odé 1979b; Dutta and Sheriff 1979): in the derivation of the impedance Z_1 and Z_2 , the plane-wave modulus M should be replaced by the bulk modulus K .

Here, we found that the original and the corrected White's models fail to predict the velocity of the partially saturated media in the absence of gas. The reason of this failure is that White's model has an implicit gas saturation assumption in the calculation of coefficients K_1 , K_2 . Consider the application of a pressure P_0 at the outer boundary, resulting in a pressure P_i at the inner boundary. The outer and inner media are characterized by Young's modulus E and Poisson's ratio σ . White assumed that the central sphere is saturated with a gas that is very light and compressible that the contribution of the inner gas sphere to the plane-wave modulus can be neglected. The Poisson's ratio of the inner sphere (containing gas) in White's original work is (White 1975):

$$\sigma_1 = \frac{\bar{M} - 2\bar{N}}{2(\bar{M} - \bar{N})}. \quad (26)$$

Here, the plane-wave modulus \bar{M} and shear modulus \bar{N} are those of the dry skeleton, ignoring the existence of gas.

This expression of the plane-wave modulus is not valid when the inner sphere is saturated with a liquid such as oil. The assumption of light and compressible inner fluid fails in this case. In order to include the contribution of the inner liquid, we compute the Poisson's ratio of the inner fluid by replacing (\bar{M}, \bar{N}) by (M_1, N_1) :

$$\sigma_1 = \frac{M_1 - 2N_1}{2(M_1 - N_1)}, \quad (27)$$

where

$$M_1 = K_1 + \frac{4}{3}N_1, \quad (28)$$

$$K_1 = \bar{K} + \frac{(1 - \bar{K}/K_s)^2}{(\phi/K_{f_1} + (1 - \phi)/K_s - \bar{K}/K_s^2)}. \quad (29)$$

In these expressions, \bar{K} is the bulk modulus of the dry frame, and K_1 is the bulk modulus of the porous rock saturated with the inner fluid. N_1 is the shear modulus of the porous rock.

The same problem occurs for the effective density (equation 12 in White's paper):

$$\rho^* = \rho_0 = (1 - \phi)\rho_s + \phi(1 - S_{f_1})\rho_{f_2} + \phi S_{f_1}\rho_{f_1}, \quad (30)$$

where S_{f_1} and S_{f_2} are the pore-space saturations of the difference types of fluids. The subscripts f_1 , f_2 represent the

Table 1 Rock properties.

Property	Value
ϕ	0.15
K_s (GPa)	35.00
ρ_s (kg/m ³)	2650
K_b (GPa)	7.00
N (GPa)	9.00
κ_{water} (m ²)	1×10^{-13}
ρ_{water} (GPa)	2.25
η_{water} (kg/m ³)	990
K_{water} (PaS)	1×10^{-3}
K_{gas} (Pa)	1×10^5
ρ_{gas} (kg/m ³)	100
η_{gas} (PaS)	1×10^{-5}
R^* (cm)	25

*All rock parameters are from (Toms *et al.* 2006).

inner and outer fluids. In this way, we can obtain the velocity and quality factor when the inner fluid is a liquid. Specific examples (oil-brine) are shown in the succeeding section.

Johnson (2001) proposed a simple closed-form analytic form of the dynamic bulk modulus

$$K^*(\omega) = K_{BGH} - \frac{K_{BGH} - K_{BGW}}{1 - \zeta + \zeta\sqrt{1 - i\omega\tau/\zeta^2}}, \quad (31)$$

where τ , ζ are functions related to the skeleton bulk modulus, porosity, saturation, fluid viscosity, and permeability. Following Johnson's original work, we list the definitions of τ , ζ in Appendix B. These functions are carefully constructed to be consistent with the BGW and BGH limits.

ATTENUATION AND DISPERSION

We calculate the P -wave velocity and attenuation based on the material properties (Toms *et al.* 2006) shown in Table 1. The numerical example shows the P -wave velocity dispersion (Figure 2) and attenuation (Figure 3) calculated with the BR method compared with those of White's and Johnson's models.

We keep all the parameters consistent with the original work. The rock parameters, including inclusion radius of 25 cm, are based on (Toms *et al.* 2006).

The wave velocities converge to the Biot-Gassmann-Wood theory limit at zero frequency, whereas at high frequencies, the velocities approach the Biot-Gassmann-Hill limit. At intermediate frequencies, a transition can be observed, which is caused by the presence of the mesoscopic patches.

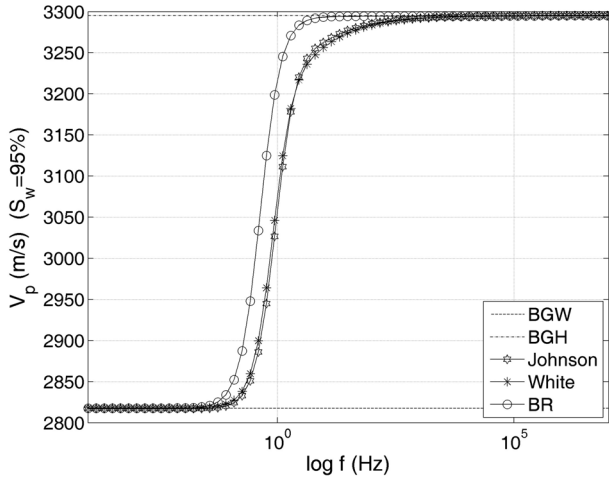


Figure 2 P-wave dispersion as a function of frequency, corresponding to the different models. Water saturation is 95%.

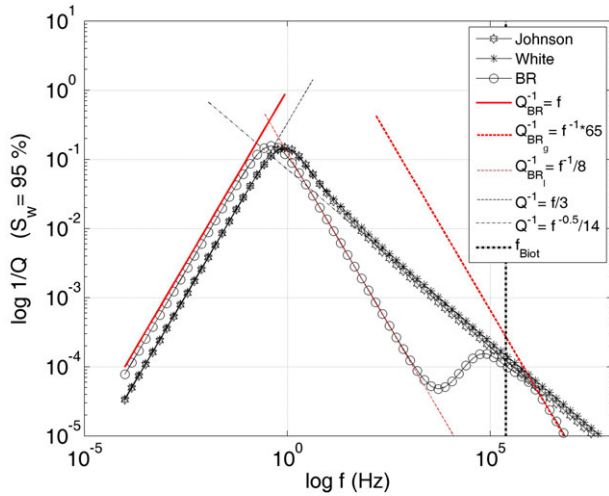


Figure 3 P-wave attenuation as a function of frequency, corresponding to the different models. Water saturation is 95%. The vertical dash-dot line represents Biot characteristic frequency $f_{\text{Biot}} = 2.4112$ kHz.

The frequency-dependent velocity transition is located between $f_l = 0.1$ Hz and $f_b = 100$ Hz. The transition of the Biot-Rayleigh theory occurs at lower frequencies, indicating higher sensitivity to the mesoscopic heterogeneity in the low-frequency band.

In this case, the diffusion wavelengths at f_l and f_b are approximately $\lambda_l = 110$ cm and $\lambda_b = 2.5$ cm. Since the patch size of the fluid heterogeneity, i.e., $R_p = 25$ cm, is smaller than λ_l , there is enough time for the fluid to flow and equilibrate the induced pressure differences at low frequencies, and the velocities approach the BGW limit. When the wave frequency

is sufficiently high, e.g., $f > f_b$, the patch size R_p is much larger than λ_b , and the velocities approach the BGH limit.

The attenuation curves calculated in this example show opposite behaviours in different frequency ranges. When the frequency is below a transition frequency f_t , the attenuation is a linear function of frequency. The asymptote is $\log_{10} Q^{-1} = a \log_{10} f + b$. Here a is the slope, and b is a constant. When the frequency is higher than f_t , the asymptote slope is -0.5 for White's and Johnson's models. The BR model has an asymptote slope $a \approx -1.0$ before a small attenuation peak (Biot dissipation). Then, the BR asymptote slope approaches that of White's and Johnson's models near the Biot dissipation peak. At the high frequency limit, the BR asymptote slope is again $a \approx -1.0$.

The large BR peak represents local fluid flow attenuation, and the smaller one indicates the Biot global flow attenuation. Johnson's model is valid for $f \ll f_{\text{Biot}}$, where the Biot crossover frequency is $f_{\text{Biot}} = \frac{\eta\phi}{2\pi\kappa\rho_f\alpha_\infty}$ (Johnson 2001). Here α_∞ is the tortuosity. The dispersion/attenuation of the fast compressional and shear waves related to Biot friction are explicitly neglected in Johnson's theory. That is the reason why the Biot attenuation peak is missing.

BR model incorporates two mechanisms: (i) local flow and (ii) Biot global flow. For certain frequencies, the two peaks may overlap. However, the two mechanisms are different. The most interesting result is that the BR local flow peak scales differently at high frequencies as compared with Johnson's model (see asymptote Q_{BR}^{-1} in Figure 3). We interpret this difference as follows.

- Johnson's asymptote slope $f^{-0.5}$ represents a sharp contrast between the fluid patch and the background medium. "Sharp" means that the length scale over which the induced pressure gradient exists is small compared with the diffusion wavelength (wavelength of the Biot slow P -wave).
- In the BR model local flow, the dependence f^{-1} means that the length scale over which the pressure gradient exists is larger than the diffusion wavelength.

Both (a) and (b) are physically possible saturation scenarios in rocks. It depends on the particular rock which scenario is more applicable. For example, in rocks where there are many small capillaries, it may be possible that there is a smooth transition from regions with 100% saturation to regions with no saturation. In such a case, the BR model takes into account that feature and therefore provides a more suitable dispersion/attenuation mechanism.

Another interesting point is that Johnson's curve seems to connect the low and high frequency peaks of the BR theory. In this theory, the local flow peak and the Biot peak represent two different mechanisms at different frequency ranges, so that the two peaks occur in different bands. If we connect the two peaks, the asymptote slope in the intermediate band behaves approximately as $1/\sqrt{f}$, meaning that the two mechanisms apply in this intermediate band. Actually, there is a small change in the descending slope near the right side of the attenuation peak in White's and Johnson's curves, which may be a transition. The BR theory is very promising in providing a precise description of the dissipation mechanism at intermediate scales, rather than describing an average effect by means of a connecting line between the low and high frequency limits.

Although the numerical predictions are nearly the same for all the models, the theoretical foundations are quite different. In this work, the differences between White's model, Johnson's model, and the BR model are clearly demonstrated.

i For White's model, the P -wave velocity is obtained as the square root of the complex bulk modulus divided by the density $v_p^* = \frac{\sqrt{K^* + \frac{4}{3}N^*}/\rho^*}{\cos(\theta_p^*/2)}$. The main contribution of White's theory is the way how the complex bulk modulus K^* is derived.

On the outer surface of concentric spheres, a specified fractional volume change is imposed at a low frequency. The resulting pressure amplitude at the surface is computed. The gas pocket provides a complete pressure release when the fluid flow in the spherical shell is included. The complex bulk modulus can be obtained by the ratio of pressure amplitude to the fractional volume change. In brief, the velocity is predicted by considering the concentric spheres as an effective homogeneous model.

ii In Johnson's model, the complex bulk modulus is derived with the branch function method within the context of the quasistatic Biot theory. A simple closed-form analytical model is proposed in the complex ω -plane as $K^*(\omega) = K_{BGH} - \frac{K_{BGH} - K_{BGW}}{1 - \zeta + \zeta \sqrt{1 - i\omega\tau/\zeta^2}}$. It is obviously some kind of interpolation between the high- and low-frequency bulk modulus K_{BGH} , K_{BGW} .

iii In the BR model, the complex P -wave is expressed as $v = \omega/k$. The relation between frequency ω and wavenumber k is obtained from the Christoffel equation, which is derived through the kinetic energy T , potential energy W , dissipation energy D , and Lagrangian formulation of the equations of motion. The approach is based on a physical theory describing the local fluid flow mechanism.

Table 2 Rock properties used in ultrasonic wave dispersion calculation.

Parameter	Values
ϕ	0.167
K_s (GPa)	37
ρ_s (kg/m ³)	2650
ρ_0 (kg/m ³)	2200
V_p (m/s)	2450
V_s (m/s)	1840
κ_{water} (D)	7.26×10^{-3}
K_{water} (GPa)	2.25
ρ_{water} (kg/m ³)	1000
η_{water} (PaS)	0.001
K_{gas} (GPa)	0.050
ρ_{gas} (kg/m ³)	1200
η_{gas} (PaS)	1.00×10^{-7}
R_p^* (mm)	0.2

* All rock parameters are from (Lebedev *et al.* 2009) except R_p , which is selected in this study.

LABORATORY DATA MODELING

Gas–water-saturated Casino sandstone

Ultrasonic velocities versus water saturation for the Casino Otway basin sandstone from quasistatic and dynamic saturation experiments have been obtained by Lebedev *et al.* (2009). The P -wave dispersion and attenuation are calculated with different models at a given frequency (1 MHz) as in the experiments. The curves depend on saturation, frequency, and water patch size. The rock parameters from (Lebedev *et al.* 2009) are used in the calculation (Table 2). The patch size is selected in this study.

The results have a consistent increasing trend bounded by the BGW and BGH limits (Figure 4). However, even at the same frequency, porosity, and saturation, the P -wave dispersion changes as the patch size changes. As in White (1975) and Dutta and Odé (1979a, b), the gas-filled regions are spherical, and all have the same radius R . The cube is approximated by a sphere with radius R_p , which has the same volume. The gas saturation S_{gas} in the spherical unit cell is the same as that in the original cubical cell, i.e., $S_{gas} = (R/R_p)^3$. When patch size R_p is fixed, the gas saturation can be determined by varying R .

The diffusion length in the experimental data is of the order of 0.1 mm (Lebedev *et al.* 2009). When a comparable patch size $R_p = 0.2$ mm (fitting parameter) is adopted, the experimental data can be fitted very well by the BR model. The

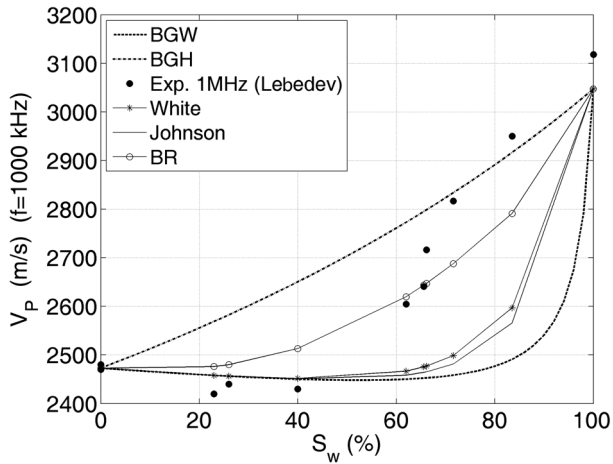


Figure 4 Comparison between the measured and the predicted P-wave velocities in Casino Otway basin sandstone. The experimental data and BGW and BGH curves are shown.

mesoscopic fluid flow due to the heterogeneities is responsible for the significant attenuation. The heterogeneities occur on a scale greater than the pore size but smaller than the wavelength. For a porous rock having only heterogeneities due to the saturating fluids, the distribution of fluid pressures is governed by the diffusion equation with a diffusion length λ_d . When λ_d is less than the patch size, the BGH bound is expected. On the contrary, if λ_d is larger than the patch size, the velocities follow the BGW prediction. The transition between these two bounds occurs when λ_d is comparable to the patch size.

Oil-brine-saturated Vosgian sandstone

The velocity of sound in French Vosgian sandstone saturated with oil and brine has been obtained by Bacri and Salin (1986). This sandstone has an average porosity of 21%. The saturations are achieved by imbibition and drainage methods. In drainage, the sandstone is fully saturated with water, and then oil is injected into the sample. The increase in oil content will cease at an irreducible water saturation of around 33%. In imbibition, the sample is fully saturated with oil. Then, small amounts of water are injected into the sample until a residual oil saturation of 35% is achieved. The sound velocities are measured at 350 kHz.

The rock parameters reported by Bacri and Salin (1986) are used in the calculation (Table 3). The patch size is selected in this study.

In the case of drainage, the measured velocities have a consistent increasing trend bounded by the BGW and BGH

Table 3 French Vosgian sandstone properties.

Property	Value
ϕ	0.21
K_s (GPa)	37
ρ_s (kg/m ³)	2650
V_p (m/s)	2050
V_s (m/s)	1240
κ (D)	0.11
V_p water (m/s)	1550
ρ_{water} (kg/m ³)	1015
η_{water} (PaS)	0.001
V_p oil (m/s)	1275
ρ_{oil} (kg/m ³)	755
η_{gas} (PaS)	0.076
R_p^* (mm)	1

* All rock parameters are from (Bacri and Salin 1986) except R_p , which is selected in this study.

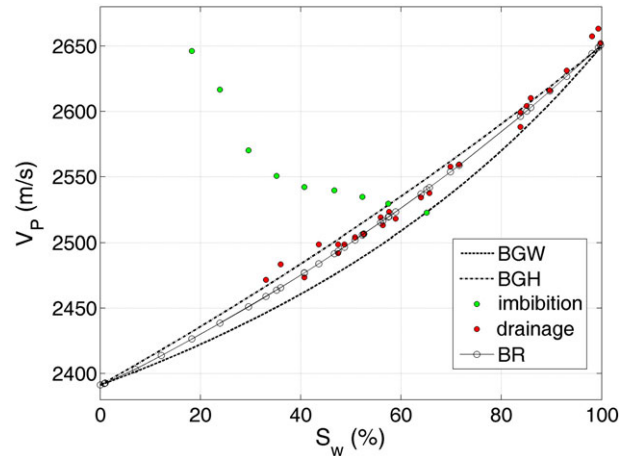


Figure 5 Comparison between the measured and the predicted P-wave velocities in Vosgian sandstone as a function of water saturation.

limits (Figure 5). When a patch size $R_p=1.0$ mm is used, the experimental data compare very well with the BR model. In general, the predicted velocities by the BR model are in good agreement with the measured data.

The imbibition velocities are very different from the drainage values. Although the velocity of sound greatly decreases as in the case of drainage, the velocity at full oil saturation is nearly the same of that at full water saturation. The effect of grain contact and surface energy on frame moduli was discussed by Bacri and Salin (1986). When the sample is immersed in water, the surface energy greatly decreases, and the frame moduli soften, and the compressional velocity decreases from 2400 m/s to 2050 m/s. When the sample is

Table 4 Properties of Estailades limestone.

Property	Value
ϕ	0.30
K_s (GPa)	76.8
ρ_s (kg/m ³)	2710
K_b (GPa)	7.45
N (GPa)	6.09
κ (D)	0.225
K_{water} (GPa)	2.25
ρ_{water} (kg/m ³)	997
η_{water} (PaS)	0.001
K_{gas} (GPa)	1.44×10^{-5}
ρ_{gas} (kg/m ³)	1240
η_{gas} (PaS)	1.0×10^{-5}
R_p^* (mm)	1.05

* All rock parameters are from (Cadoret *et al.* 1995) except R_p , which is selected in this study.

immersed in oil, the surface energy is slightly affected. Stiffening of the rock skeleton has been observed when rock was saturated by different fluids (Cadoret *et al.* 1998). In this example, full oil saturation leads to a wave velocity larger than that of the dry value (Bacri and Salin 1986). The surface effect causes discrepancies between the imbibition data and the theoretical predictions. A detailed study of the pore–fluid influence on grain contacts and frame stiffness is required to improve the velocity models.

Gas–water-saturated Estailades limestone

Elastic wave velocities in homogeneous limestone were measured in the laboratory in three different frequency ranges with varying water saturations by Cadoret *et al.* (1995). Eight different quarry limestones covering a wide range of porosities and permeabilities were chosen for the sonic and ultrasonic experiments. The P -wave velocity of Estailades limestone of approximately 30% porosity and a permeability of 225 mD has been obtained. Measurements were obtained using large resonant bars at frequencies of approximately 1 kHz. The conventional pulse transmission technique was used at 500 kHz. The sample was saturated using drainage and imbibition techniques (Cadoret *et al.* 1995), and the P -wave velocities were measured at 1 kHz and 500 kHz.

The rock porosity and permeability used in the calculation (Table 4) are obtained from (Cadoret *et al.* 1995). The mineral properties are obtained from (Mavko *et al.* 2009). The patch size is selected in this study. The bulk modulus

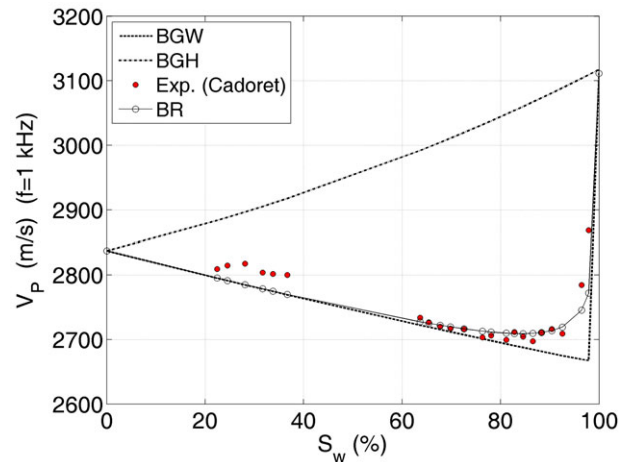


Figure 6 Comparison between the measured and predicted P -wave velocities for Estailades limestone as a function of gas–water saturation. The porosity is 0.30, and the frequency is 1 kHz.

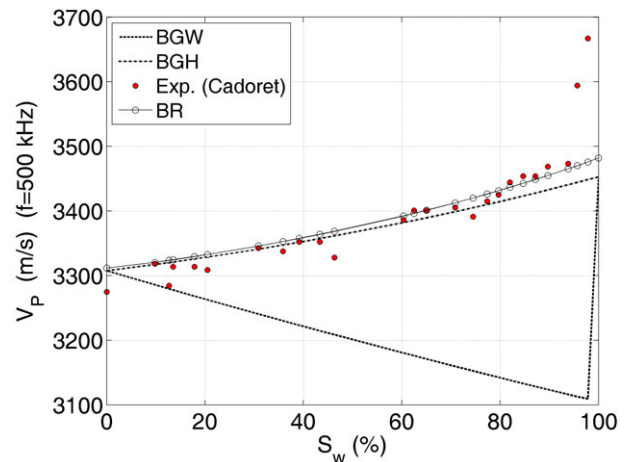


Figure 7 Comparison between the measured and predicted P -wave velocities for Estailades limestone as a function of gas–water saturation. The porosity is 0.30, and the frequency is 500 kHz.

K_b and shear modulus N are estimated from the measured P -wave and S -wave velocities for dry rocks (Cadoret *et al.* 1995). With these parameters, we calculated $V_p(S_w)$ for all the models at 1 kHz (Figure 6) and 500 kHz (Figure 7).

In Figure 6, the experimental data (see Figs. 3 and 7 in Cadoret *et al.* 1995) and predicted velocities are bounded by the BGW and BGH limits. In addition, the velocities are close to the low-frequency velocity limit (BGW). There is a sudden decrease in velocity when water saturation decreases from 100% to 95%. As gas saturation increases, the velocity gradually increases. Beyond 60% water saturation, the BR model provides the best prediction of the experimental data.

The velocity curves of the BR model are calculated as a function of given parameters. These are: ϕ_{m0} , K_s , N , K_f , K_b , ρ_s , ρ_f , κ ($m=1,2$), η , patch size R_p , and wave frequency ω . The porosity in each phase is ϕ_{m0} . The frame bulk modulus is K_b , and the solid and fluid bulk moduli are K_s , K_f . N is the shear modulus of the frame. Here ρ_s , ρ_f are mineral grain density and fluid density. κ is the permeability, and η is the fluid viscosity. The basic parameters for the mineral, fluids, and dry rock are taken from (Cadoret *et al.* 1995) and (Mavko *et al.* 2009). Actually, the real patch size is difficult to measure, and in most cases, there are no spherical patches. All the models are based on idealized geometries, and the patch size can be an adjustable parameter.

Figure 7 indicates that the experimental data are close to the high frequency limit (BGH). At low S_w , the predicted data are very close to the experimental data. When S_w approaches 100%, the experimental velocity greatly increases. All the models, including the BGH limit, underestimate the P-wave velocity at full water saturation. At high water saturation, the BR model predictions are closer to the measured data.

CONCLUSIONS

The purpose of this work is to quantitatively analyze the performance of the main patchy-saturation models in predicting the P-wave velocity dispersion/attenuation in real rocks. The BR, White's, and Johnson's models are derived from different principles, the dispersion/attenuation trends of which are similar but predictions are slightly different for partially saturated media. Minor differences have been observed: (i) Johnson's model is robust and performs better in general, (ii) White's model provides similar results to Johnson's model but fails in the case of oil-water saturation, and (iii) only the BR model describes both the local- and global-flow dissipation mechanisms. White's model is extended here to the case of liquid-liquid saturations (such as oil-water), based on a modification of the Poisson's ratio and the effective density. Numerical/experimental data comparisons illustrate that by using the Johnson's and modified White's models, the predicted P-wave velocities are approximately the same. The BR predicted velocity is slightly higher than that of the Johnson's and White's models. In tight sandstones, this velocity prediction agrees with the data, particularly for water saturations between 30% and 70%. For limestone with a porosity of $\phi = 0.3$, the BR model predicts the velocities at both the sonic and ultrasonic ranges. The local-flow dissipation peak of the BR model scales differently at high frequencies com-

pared with the Johnson's and White's models. This difference may be due to the saturation contrast between the fluid patch and the background medium. In the case of a smooth saturation transition, the BR model may provide a more reliable dispersion/attenuation description.

ACKNOWLEDGEMENTS

We thank Dr. David L. Johnson for providing the source code of P-wave dispersion and attenuation. This research was sponsored by NNSF of China (41104066), by the Open Foundation of SINOPEC Key Laboratory of Geophysics, by RIPED Youth Innovation Foundation (2010-A-26-01), and by the 12th 5-Year Basic Research Program of CNPC (2011A-3601). J.M. Carcione would like to thank the CO2 Monitor Project.

REFERENCES

- Achenbach J. 1987. *Wave Propagation in Elastic Solids*. North Holland Publishing, Amsterdam.
- Ba J., Cao H., Carcione J.M., Tang G., Yan X.F., Sun W.T. *et al.* 2013. Multiscale rock-physics templates for gas detection in carbonate reservoirs. *Journal of Applied Geophysics* 93, 77–82.
- Ba J., Carcione J.M., Cao H., Du Q.Z., Yuan Z.Y. and Lu M.H. 2012. Velocity dispersion and attenuation of P waves in partially-saturated rocks: wave propagation equations in double-porosity medium. *Chinese Journal of Geophysics* 55, 219–231.
- Ba J., Carcione J.M. and Nie J.X. 2011. Biot-Rayleigh theory of wave propagation in double-porosity media. *Journal of Geophysical Research* 116, B06202.
- Ba J., Nie J.X., Cao H. and Yang H.Z. 2008. Mesoscopic fluid flow simulation in double-porosity rocks. *Geophysical Research Letter* 35, L04303.
- Bacri J.-C. and Salin D. 1986. Sound velocity of a sandstone with oil and brine at different concentrations. *Geophysical Research Letters* 13, 326–328.
- Berryman J.G. 1979. Theory of elastic properties of composite materials. *Applied Physics Letters* 35, 856–858.
- Berryman J.G. 1980. Confirmation of Biot's theory. *Applied Physics Letters* 37, 382–384.
- Biot M.A. 1962. Mechanics of deformation and acoustic propagation in porous media. *Journal of Applied Physics* 33, 1482–1498.
- Cadoret T., Marion D. and Zinszner B. 1995. Influence of frequency and fluid distribution on elastic wave velocities in partially saturated limestones. *Journal of Geophysical Research* 100, 9789–9803.
- Cadoret T., Mavko G. and Zinszner B. 1998. Fluid distribution effect on sonic attenuation in partially saturated limestones. *Geophysics* 63, 154–160.
- Carcione J.M. 2007. *Wave Fields in Real Media: Theory and Numerical Simulation of Wave Propagation in Anisotropic, Anelastic, Porous and Electromagnetic Media*. Elsevier.

- Carcione J.M. and Helle H.B. 2002. Rock physics of geopressure and prediction of abnormal pore fluid pressures using seismic data. *CSEG Recorder* 27, 8–32.
- Carcione J.M. and Picotti S. 2006. P-wave seismic attenuation by slow-wave diffusion: effects of inhomogeneous rock properties. *Geophysics* 71, O1–O8.
- Caspari E., Müller T.M. and Gurevich B. 2011. Time-lapse sonic logs reveal patchy CO₂ saturation in-situ. *Geophysical Research Letters* 38, L13301.
- Dutta N.C. and Odé H. 1979a. Attenuation and dispersion of compressional waves in fluid-filled porous rocks with partial gas saturation (White model).1. Biot theory. *Geophysics* 44, 1777–1788.
- Dutta N.C. and Odé H. 1979b. Attenuation and dispersion of compressional waves in fluid-filled porous rocks with partial gas saturation (White model).2. Results. *Geophysics* 44, 1789–1805.
- Dutta N.C. and Seriff A.J. 1979. On White's model of attenuation in rocks with partial gas saturation. *Geophysics* 44, 1806–1812.
- Dvorkin J., Mavko G. and Nur A. 1995. Squirt Flow in fully saturated rocks. *Geophysics* 60, 97–107.
- Dvorkin J. and Nur A. 1993. Dynamic poroelasticity - a unified model with the squirt and the Biot mechanisms. *Geophysics* 58, 524–533.
- Hill R. 1963. Elastic properties of reinforced solids: some theoretical principles. *Journal of the Mechanics and Physics of Solids* 11, 357–372.
- Hill R. 1964. Theory of mechanical properties of fibre-strengthened materials: I. elastic behaviour. *Journal of the Mechanics and Physics of Solids* 12, 199–212.
- Johnson D.L. 1986. Recent developments in the acoustic properties of porous media. In: *Frontiers in Physical Acoustics XCIII* (ed D. Sette), pp. 255–290. Elsevier, New York.
- Johnson D.L. 2001. Theory of frequency dependent acoustics in patchy-saturated porous media. *Journal of the Acoustical Society of America* 110, 682–694.
- Lebedev M., Toms-Stewart J., Clennell B., Pervukhina M., Shulakova V., Paterson L. et al. 2009. Direct laboratory observation of patchy saturation and its effects on ultrasonic velocities. *The Leading Edge* 28, 24–27.
- Mavko G., Mukerji T. and Dvorkin J. 2009. *The Rock Physics Handbook: Tools for Seismic Analysis of Porous Media*. Cambridge University Press.
- Müller T.M. and Gurevich B. 2004. One-dimensional random patchy saturation model for velocity and attenuation in porous rocks. *Geophysics* 69, 1166–1172.
- Müller T.M., Gurevich B. and Lebedev M. 2010. Seismic wave attenuation and dispersion resulting from wave-induced flow in porous rocks – a review. *Geophysics* 75, A147–A164.
- Rayleigh L. 1917. On the pressure developed in a liquid during the collapse of a spherical cavity. *Philosophical Magazine* 34, 94–98.
- Ruiz F. and Ilgar Azizov R. 2011. Fluid substitution in tight shale using the soft-porosity model. 81st SEG annual meeting, San Antonio, USA, 2272–2276.
- Sun W., Ba J., Müller T.M., Carcione J.M., Cao H., Du Q. et al. 2012. P-Wave dispersion and attenuation in patchy-saturated rocks: White, Dutta, Johnson and Biot-Rayleigh theories. 74th EAGE in Copenhagen, Copenhagen, Denmark.
- Toms J., Müller T.M., Ciz R. and Gurevich B. 2006. Comparative review of theoretical models for elastic wave attenuation and dispersion in partially saturated rocks. *Soil Dynamics and Earthquake Engineering* 26, 548–565.
- Toms J., Müller T.M. and Gurevich B. 2007. Seismic attenuation in porous rocks with random patchy saturation. *Geophysical Prospecting* 55, 671–678.
- White J.E. 1975. Computed seismic speeds and attenuation in rocks with partial gas saturation. *Geophysics* 40, 224–232.
- White J.E., Mikhaylova N.G. and Lyakhovitskiy F.M. 1975. Low-frequency seismic waves in fluid-saturated layered rocks. *The Journal of the Acoustical Society of America* 57, S30.
- Wood A.B. 1955. *A Textbook of Sound; Being an Account of the Physics of Vibrations with Special Reference to Recent Theoretical and Technical Developments*. Macmillan, New York.

APPENDIX A

WHITE'S MODEL: RELEVANT EQUATIONS

$$K_0 = \bar{K}_3 / (\bar{K}_2 - \bar{K}_1) \quad (\text{A1})$$

$$\mathfrak{R}_1 = \frac{K_{f_1}}{\phi} \left[\frac{(1 - K_1/K_{s_1})}{(1 - K_{f_1}/K_{s_1})} \right] \frac{\bar{K}_1}{K_1}, \quad (\text{A2})$$

$$\mathfrak{R}_2 = \frac{K_{f_2}}{\phi K_2} \left[\frac{(1 - K_2/K_{s_2})(1 - S_G \bar{K}_1)}{(1 - K_{f_2}/K_{s_2})(1 - S_G)} \right], \quad (\text{A3})$$

$$\Theta_1 = (1 - \bar{K}/K_s) \frac{K_{A_1}}{K_1}, \quad (\text{A4})$$

$$\Theta_2 = (1 - \bar{K}/K_s) \frac{K_{A_2}}{K_2}, \quad (\text{A5})$$

$$Z_1 = \frac{\eta_1 a}{\kappa_1} \left[\frac{1 - e^{-2\alpha_1 a}}{(\alpha_1 a - 1) + (\alpha_1 a + 1) e^{-2\alpha_1 a}} \right], \quad (\text{A6})$$

$$Z_2 = \frac{\eta_2 a}{\kappa_2} \left[\frac{(\alpha_2 b + 1) + (\alpha_2 b - 1) e^{2\alpha_2(b-a)}}{(\alpha_2 b + 1)(\alpha_2 a - 1) - (\alpha_2 b - 1)(\alpha_2 a + 1) e^{2\alpha_2(b-a)}} \right] \quad (\text{A7})$$

$$\alpha_1 = (\omega \eta_1 / \kappa_1 K_{E1})^{1/2}, \quad (\text{A8})$$

$$\alpha_2 = (\omega \eta_2 / \kappa_2 K_{E2})^{1/2}, \quad (\text{A9})$$

$$K_{E1} = \left(1 - \frac{K_{f_1} (1 - K_1/K_s) (1 - \bar{K}/K_s)}{\phi K_1 (1 - K_{f_1}/K_s)} \right) K_{A_1}, \quad (\text{A10})$$

$$K_{E2} = \left(1 - \frac{K_{f2}(1 - K_2/K_s)(1 - \bar{K}/K_s)}{\phi K_2(1 - K_{f2}/K_s)} \right) K_{A2}, \quad (\text{A11})$$

where K_{f1} and K_{f2} are fluid bulk moduli; ϕ is porosity; η , κ are viscosity and permeability, respectively; K_s is the solid bulk modulus; and subscripts 1 and 2 refer to the inner sphere and concentric shell, respectively. In the situation of a single-porosity solid saturated with two immiscible fluids, $\kappa_1 = \kappa_2 = \kappa$. The gas saturation is $S_G = a^3/b^3$, where a , b are the radii of the inner sphere and the concentric shell, respectively. The parameters \bar{K}_1 , \bar{K}_2 , \bar{K}_3 , K_1 , K_2 , K_{A1} , K_{A2} are defined as:

$$\bar{K}_1 = \frac{3(1 - \sigma_2)/2}{(1 - 2\sigma_1)(1 - S_G)E_2/E_1 + S_G(1 - 2\sigma_2) + (1 + \sigma_2)/2}. \quad (\text{A12})$$

$$\bar{K}_2 = \frac{(1 - 2\sigma_2)/S_G + (1 + \sigma_2)/2}{3(1 - \sigma_2)/2}, \quad (\text{A13})$$

$$\bar{K}_3 = \frac{E_2(1/S_G - 1)}{3(1 - 2\sigma_2) + 3(1 + \sigma_2)/2}, \quad (\text{A14})$$

$$K_m = \bar{K} + \frac{(1 - \bar{K}/K_s)^2}{(\phi/K_{f_m} + (1 - \phi)/K_s - \bar{K}/K_s^2)}, \quad m = 1, 2, \quad (\text{A15})$$

$$K_{A_m} = \left(\frac{\phi}{K_{f_m}} + \frac{1 - \phi}{K_s} - \frac{\bar{K}}{K_s^2} \right)^{-1}, \quad m = 1, 2, \quad (\text{A16})$$

where E and σ are Young's modulus and Poisson's ratio, respectively, and \bar{K} is the bulk modulus of skeleton.

APPENDIX B

JOHNSON'S MODEL: RELEVANT EQUATIONS

$$\tau = \left[\frac{K_{BGH} - K_{BGW}}{K_{BGH}G} \right]^2 \quad (\text{B1})$$

$$\zeta = \frac{(K_{BGH} - K_{BGW})^3}{2K_{BGW}K_{BGH}^2TG^2} = \frac{(K_{BGH} - K_{BGW})}{2K_{BGW}} \cdot \frac{\tau}{T} \quad (\text{B2})$$

$$T = \frac{K_{BGW}\phi^2}{30\kappa b^3} \{ [3\eta_2g_2^2 + 5(\eta_1 - \eta_2)g_1g_2 - 3\eta_1g_1^2] a^5 - 15\eta_2g_2(g_2 - g_1)a^3b^2 + 5g_2[3\eta_2g_2 - (2\eta_2 + \eta_1)g_1]a^2b^3 - 3\eta_2g_2^2b^5 \} \quad (\text{B3})$$

$$g_m = \frac{(1 - K_b/K_s)(1/K_W - 1/K_{f_m})}{(1 - K_b/K_s - \phi K_b/K_s + \phi K_b/K_W)} \quad (\text{B4})$$

$$G = \left| \frac{\Delta p_f}{P_e} \right|^2 \cdot \frac{S}{V} \cdot \frac{i}{q^*} (-i\omega)^{1/2} \quad (\text{B5})$$

$$\frac{\Delta p_f}{P_e} = \frac{(R_2 + Q_2)[K_1 + (4/3)N] - (R_1 + Q_1)[K_2 + (4/3)N]}{\phi S_1 K_2 [K_2 + (4/3)N] + \phi S_2 K_2 [K_1 + (4/3)N]} \quad (\text{B6})$$

$$K_m = \frac{K_s + [\phi(K_s/K_{f_m}) - \phi - 1]K_b}{1 - \phi - (K_b/K_s) + \phi(K_s/K_{f_m})}, \quad m = 1, 2, \quad (\text{B7})$$

$$S/V = 3a^2/b^3 \quad (\text{B8})$$

$$q^* = \sqrt{i\omega/D^*}. \quad (\text{B9})$$

$$D^* = \left[\frac{\kappa K_{BGH}}{\eta_1\sqrt{D_1} + \eta_2\sqrt{D_2}} \right]^2. \quad (\text{B10})$$

$$D_m = \frac{\kappa K_{f_m}}{\eta_m\phi} \left\{ 1 + \frac{K_{f_m}}{\phi[K_b + (4/3)N]} \left\{ 1 + \frac{1}{K_s} \left[\frac{4}{3}N \left(1 - \frac{K_b}{K_s} \right) - K_b - \phi \left(K_b + \frac{4}{3}N \right) \right] \right\} \right\}^{-1}, \quad m = 1, 2, \quad (\text{B11})$$

where Δp_f is the discontinuity in pore pressure across the concentric sphere interface S ; P_e is the applied external stress; V is sample volume; a and b are the radii of the inner sphere and the concentric shell, respectively; ϕ is porosity; and η and κ are viscosity and permeability, respectively. The parameters P , Q , R are:

$$P_m = \frac{(1 - \phi)[1 - \phi - K_b/K_s]K_s + \phi(K_s/K_{f_m})K_b}{1 - \phi - K_b/K_s + \phi K_s/K_{f_m}} + \frac{4}{3}N, \quad m = 1, 2, \quad (\text{B12})$$

$$Q_m = \frac{(1 - \phi - K_b/K_s)\phi K_s}{1 - \phi - K_b/K_s + \phi K_s/K_{f_m}}, \quad m = 1, 2, \quad (\text{B13})$$

$$R_m = \frac{\phi^2 K_s}{1 - \phi - K_b/K_s + \phi K_s/K_{f_m}}, \quad m = 1, 2, \quad (\text{B14})$$

where K_s is the solid phase bulk modulus, N is the solid phase shear modulus, K_b is the porous skeleton bulk modulus, and K_f is the pore fluid bulk modulus. The effective modulus of pore fluid given by Wood's law (Wood 1955) for two liquids is $K_W = \left(\frac{S_1}{K_{f1}} + \frac{S_2}{K_{f2}} \right)^{-1}$, where S_1 , S_2 are saturations of the liquids.